Adaptive evolution shapes the present-day distribution of the thermal sensitivity of population growth rate

Dimitrios - Georgios Kontopoulos[1,2*], Thomas P. Smith[2], Timothy G. Barraclough[2], Samraat Pawar[2]

1 Science and Solutions for a Changing Planet DTP, Imperial College London, London, United Kingdom
2 Department of Life Sciences, Imperial College London, Silwood Park, Ascot, Berkshire, United Kingdom

* dgkontopoulos@gmail.com

Abstract

Developing a thorough understanding of how ectotherm physiology adapts to different thermal environments is of crucial importance, especially in the face of global climate change. A key aspect of an organism's thermal performance curve—the relationship between fitness-related trait performance and temperature—is its thermal sensitivity, i.e., the rate at which trait values increase with temperature within its typically-experienced thermal range. For a given trait, the distribution of thermal sensitivities across species, often quantified as "activation energy" values, is typically right-skewed. Currently, the mechanisms that generate this distribution are unclear, with considerable debate about the role of thermodynamic constraints vs adaptive evolution. Here, using a phylogenetic comparative approach, we study the evolution of the thermal sensitivity of population growth rate across phytoplankton (Cyanobacteria and eukaryotic microalgae) and prokaryotes (bacteria and archaea), two microbial groups that play a major role in the global carbon cycle. We find that thermal sensitivity across these groups is moderately phylogenetically heritable, and that its distribution is shaped by repeated evolutionary convergence throughout its parameter space. More precisely, we detect bursts of adaptive evolution in thermal sensitivity, increasing the amount of overlap among its distributions in different clades. We obtain qualitatively similar results from evolutionary analyses of the thermal sensitivities of two physiological rates underlying growth rate: net photosynthesis and respiration of plants. Furthermore, we find that these episodes of evolutionary convergence are partly driven by two opposing forces: decrease in thermal sensitivity due to environmental fluctuations and increase due to adaptation to stable environments. Overall, our results indicate that adaptation can lead to large and relatively rapid shifts in thermal sensitivity, especially in microbes where rapid evolution can take place at ecological time scales. Thus, more attention needs to be paid to elucidating the implications of rapid evolution in organismal thermal sensitivity for ecosystem functioning.

Author summary

Changes in environmental temperature influence the performance of biological traits (e.g., respiration rate) in ectotherms, with the relationship between trait performance and temperature (the "thermal performance curve") being single-peaked. Understanding

how thermal performance curves adapt to different environments is important for predicting how organisms will be impacted by climate change. One key aspect of the shape of these curves is the thermal sensitivity near temperatures typically experienced by the species. Whether and how thermal sensitivity responds to different environments is a topic of active debate. To shed light on this, here we perform an evolutionary analysis of the thermal sensitivity of three key traits of prokaryotes, phytoplankton, and plants. We show that thermal sensitivity does not evolve in a gradual manner, but can differ considerably even between closely related species. This suggests that thermal sensitivity undergoes rapid adaptive evolution, which is further supported by our finding that thermal sensitivity varies weakly with latitude. We conclude that variation in thermal sensitivity arises partly from adaptation to environmental factors and that this may need to be accounted for in ecophysiological models.

Introduction

Current climate change projections suggest that the average global temperature in 2100 will be higher than the average of 1986-2005 by 0.3-4.8°C [1], coupled with an increase in temperature fluctuations in certain areas [2]. Therefore, it is now more important than ever to understand how temperature changes affect biological systems, from individuals to whole ecosystems. At the level of individual organisms, temperature affects functional traits in the form of the "thermal performance curve" (TPC). Typically, this TPC, especially when the trait is a rate (e.g., respiration rate, photosynthesis, growth), takes the shape of a negatively-skewed unimodal curve (Fig. 1) [3, 4]. The curve increases (approximately) exponentially to a maximum (T_{pk}), and then also decreases exponentially, with the fall being steeper than the rise. Understanding how various aspects of the shape of this TPC adapt to a changing thermal environment is crucial for predicting how rapidly organisms can respond to climate change.

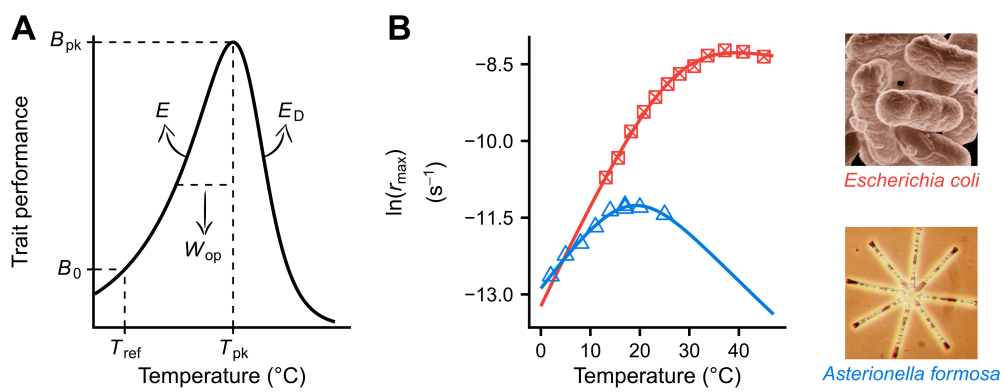

Fig 1. The thermal performance curve (TPC) of ectotherm metabolic traits, as described by the Sharpe-Schoolfield model [5]. (A) T_{pk} (K) is the temperature at which the curve peaks, reaching a maximum height that is equal to B_{pk} (in units of trait performance). E and E_{D} (eV) control how smoothly the TPC rises and falls respectively. B_0 (in units of trait performance) is the trait performance normalised at a reference temperature (T_{ref}) below the peak. In addition, W_{op} (K), the operational niche width of the TPC, can also be calculated *a posteriori* as the difference between T_{pk} and the temperature at the rise of the TPC where $B(T) = 0.5 \cdot B_{\mathrm{pk}}$. (B) TPCs of individual- and population-level traits (such as r_{max}) are usually well-described by the Sharpe-Schoolfield model.

According to the Metabolic Theory of Ecology (MTE) as well as a large body of physiological research, the shape of the TPC is expected to reflect the effects of temperature on the kinetics of a single rate-limiting enzyme involved in key metabolic reactions [5–9]. Therefore, the rise in trait values up to T_{pk} can be mechanistically described using the Boltzmann-Arrhenius equation:

$$B(T) = B_0 \cdot e^{\left[\frac{-E}{k} \cdot \left(\frac{1}{T} - \frac{1}{T_{\mathrm{ref}}}\right)\right]}. \tag{1}$$

Here, B is the value of a biological trait, B_0 is a normalisation constant—that includes the effect of cell or body size—which gives the trait value at a reference temperature (T_{ref}), T is temperature (in K), k is the Boltzmann constant ($8.617 \cdot 10^{-5}$ eV $\cdot$ K^{-1}), and E (eV) is the thermal sensitivity of the trait within the temperature range typically experienced by the individuals of the species.

Early MTE studies argued that, because of strong thermodynamic constraints, adaptation will predominantly result in changes in B_0, whereas E will remain almost constant across traits (e.g., respiration rate, r_{max}), species, and environments around a range of 0.6-0.7 eV [6–8]. The latter assumption is referred to in the literature as "universal temperature dependence" (UTD). This restricted range of values that E can take is centered on the putative mean activation energy of respiration (≈ 0.65 eV). A notable exception to the UTD is photosynthesis rate, which is expected to have a lower E value of ≈ 0.32 eV, reflecting the activation energy of the rate-limiting steps of photosynthesis [10].

The existence of a UTD has been strongly debated. From a theoretical standpoint, critics of the UTD have argued that the Boltzmann-Arrhenius model is too simple to mechanistically describe the complex physiological mechanisms of diverse organisms [3, 11–13], and is inadequate for describing TPCs emerging from the interaction of multiple factors, and not just the effects of temperature on enzyme kinetics. That is, the E calculated by fitting the Boltzmann-Arrhenius model to biological traits is an emergent property that does not directly reflect the activation energy of a single rate-limiting enzyme. For example, a fixed thermal sensitivity for net photosynthesis rate is not realistic because it depends on the rate of gross photosynthesis as well as photorespiration, which is in turn determined not only by temperature but also by the availability of CO_2 in relation to O_2 [14].

Indeed, there is now overwhelming empirical evidence for variation in E (thermal sensitivity) far exceeding the narrow 0.6-0.7 eV range [15–20], whereas the distribution of E values across species is typically not Gaussian (as expected from moderate measurement error around a fixed value) but right-skewed. Given that E is necessarily positive (i.e., its lower boundary is 0 eV), a skewed distribution could, in theory, arise from very substantial measurement error [18, 21]. In that case, however, we would expect a high density of E values close to 0 eV, but such a pattern has not been observed [15]. Both the deviations from the MTE expectation of a heavily restricted range for E and the shape of its distribution have been argued to be partly driven by adaptation to local environmental factors by multiple studies. These include selection on prey to have lower thermal sensitivity than predators (the "thermal life-dinner principle") [15], adaptation to temperature fluctuations [3, 17, 22, 23], and adaptive increases in carbon allocation or use efficiency due to warming [24–27].

In general then, adaptive changes in the TPCs of underlying (fitness-related) traits are expected to influence the TPCs of higher-order traits such as r_{max}, resulting in deviations from a UTD. Therefore, understanding how the thermal sensitivity of r_{max} and its distribution evolves is particularly important, as it may also yield useful insights about the evolution of the TPCs of underlying physiological traits (e.g., respiration rate,

photosynthesis rate, and carbon allocation efficiency). Indeed, systematic shifts in the thermal sensitivity of fundamental physiological traits have been documented, albeit not in a phylogenetic context.

In particular, the phylogenetic heritability—the extent to which closely related species have more similar trait values than species chosen at random—of thermal sensitivity can provide key insights. A phylogenetic heritability of 1 indicates that the trait evolves randomly across the phylogenetic tree following Brownian motion. In contrast, a phylogenetic heritability of 0 indicates that trait values are independent of the phylogeny either because i) the trait is practically invariant across species and any variation is due to measurement error, or ii) the evolution of the trait is very fast and with frequent convergence. Phylogenetic heritabilities between 0 and 1 reflect deviations from random evolution (e.g., due to occasional patterns of evolutionary convergence). Among phytoplankton, measures of thermal sensitivity of $r_{\max}$ (E and W_{op}) have previously been shown to exhibit intermediate phylogenetic heritability [28]. This indicates that among phytoplankton, thermal sensitivity is not constant but evolves along the phylogeny, albeit not as a purely random walk in trait space.

To understand i) how variation in thermal sensitivity accumulates across multiple autotroph and heterotroph groups, and ii) whether its distribution is shaped by environmental selection, here we conduct a thorough investigation of the evolutionary patterns of thermal sensitivity, focusing particularly on $r_{\max}$. More precisely, we first examine how variation in E and W_{op} is distributed along the phylogeny by estimating their phylogenetic heritability and examining how their disparity changes through time. Next, we investigate if clades systematically differ in their evolutionary rate for E and W_{op}. For example, the emergence of an evolutionary innovation could confer an increased evolutionary rate in thermal sensitivity, allowing species to better explore its parameter space (i.e., through large changes in E and W_{op} values). This is followed by a visualization of thermal sensitivity evolution, with which we test the aforementioned MTE assumption that thermodynamic constraints force thermal sensitivity to evolve very tightly around a global optimum (near 0.65 or 0.32 eV). Finally, we examine if thermal sensitivity systematically decreases from the equator to intermediate latitudes, as this would suggest that thermal sensitivity responds to the magnitude of fluctuations in environmental temperature.

Results

Dataset sources

We combined two pre-existing datasets of $r_{\max}$ TPCs, spanning 380 phytoplankton species (a polyphyletic group that includes prokaryotic Cyanobacteria and eukaryotic phyla such as Dinophyta) [28] and 272 prokaryote species (bacteria and archaea) [29]. In addition, we also collected two TPC datasets of traits that underlie $r_{\max}$: net photosynthesis and respiration rates of algae, aquatic and terrestrial plants (221 and 201 species respectively) [27]. We used these two smaller datasets to understand if the evolutionary patterns of thermal sensitivity differ between i) higher-order traits and ii) traits that are more tightly linked to organismal physiology. Trait values were typically measured under nutrient-, light- and CO_2-saturated conditions (where applicable), after acclimation to each experimental temperature.

To investigate the evolution of measures of thermal sensitivity across species, we reconstructed the phylogeny of as many species in the four datasets as possible, from publicly available nucleotide sequences of i) the small subunit rRNA gene from all species groups and the ii) cbbL/rbcL gene from photosynthetic prokaryotes, algae, and plants (see the Methods section). We managed to obtain small subunit rRNA gene

sequences from 537 species and cbbL/rbcL sequences from 208 of them (Tables S4 and S5 in the S1 Appendix).

TPC parameters were quantified for each species/strain present in the phylogeny using the Sharpe-Schoolfield model (see Fig. 1 and the Methods section). The resulting estimates of thermal sensitivity were found to be right-skewed (Fig. S2 in Appendix S1) as has been shown previously [15, 17]. Furthermore, we did not detect a disproportionately high density of thermal sensitivity values near the lower boundary of E (0 eV), as we would expect if all variation was due to strong measurement error around a true value of e.g., 0.65 eV. Thus, these results are not consistent with the assumption of early MTE studies that thermal sensitivity is nearly invariant.

Phylogenetic comparative analyses

We next investigated the evolutionary patterns of thermal sensitivity. Given that the main focus of this study is to investigate how the thermal sensitivity of $r_{\max}$ (a direct measure of fitness) evolves, most of the following comparative analyses were performed on our two large TPC datasets ($r_{\max}$ of phytoplankton and prokaryotes). Besides this, the sample sizes of the two smaller datasets would be inadequate for obtaining robust results for many of our analyses. If an analysis makes use of all four datasets, this is explicitly stated.

An issue that is worth mentioning is the overlap between the datasets of phytoplankton and prokaryotic TPCs, given that both of them include Cyanobacteria. To address this, we kept Cyanobacteria as part of the phytoplankton dataset (due to their functional similarity) and did not include them in analyses of prokaryotes. We also examined whether our results were mainly driven by the long evolutionary distance between Cyanobacteria and eukaryotic phytoplankton by repeating all phytoplankton analyses after removing Cyanobacteria (see subsection S3.2 in Appendix S1).

Estimation of phylogenetic heritability

As TPC parameters capture different features of the shape of the same curve, it is likely that some of them may covary [28]. To account for this in the estimation of phylogenetic heritability, we fitted a multi-response phylogenetic regression model using the MCMCglmm R package (v. 2.26) [30] in which all TPC parameters formed a combined response. The model was fitted separately to our two large TPC datasets: $r_{\max}$ of phytoplankton and prokaryotes. To satisfy the assumption of models of trait evolution that the change in trait values is normally distributed, we transformed all TPC parameters so that their distributions would be approximately Gaussian (see Fig. 2).

Non-negligible phylogenetic heritability was detected in measures of thermal sensitivity (E and W_{op}), as well as all other TPC parameters, across phytoplankton (including or excluding Cyanobacteria) and prokaryotes (Figs. 2 and S7). In particular, the phylogenetic heritability estimates of $\ln(E)$ and $\ln(W_{\mathrm{op}})$ were statistically different from both zero and one, indicating that the two TPC parameters evolve across the phylogeny but not in a purely random (Brownian motion) manner. In general, TPC parameters exhibit a similar phylogenetic heritability between the two species groups. The only major exception is $\ln(B_{\mathrm{pk}})$, which is considerably more heritable among prokaryotes than among phytoplankton. This difference in phylogenetic heritability most likely reflects the strength of the positive correlation between B_{pk} and T_{pk} (a "hotter is better" pattern) in the two groups. More precisely, T_{pk}, which has a phylogenetic heritability of ≈ 1, is more strongly correlated with B_{pk} among prokaryotes [29] than among phytoplankton [28], possibly due to the differences in their cellular physiology. For example, phytoplankton growth rate depends on the interplay among the processes of photosynthesis, respiration, as well as cell maintenance, whose

thermal sensitivities can strongly differ [27]. Overall, these results serve as further evidence that the thermal sensitivity of $r_{\max}$ varies systematically across species, beyond what would be expected purely from measurement error.

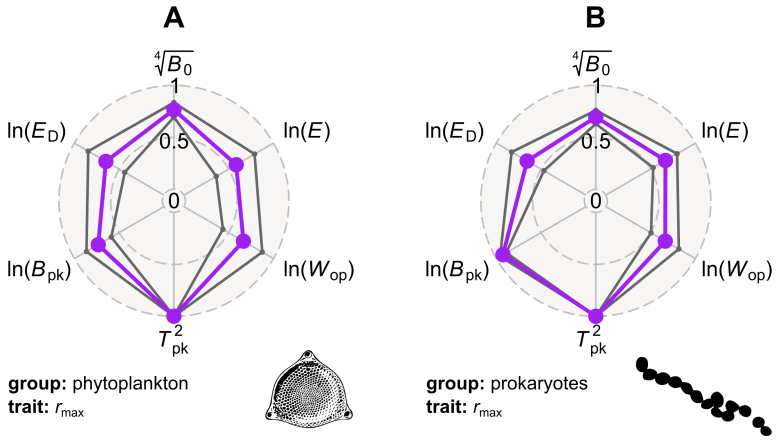

Fig 2. Moderate to strong phylogenetic heritability can be detected in all TPC parameters, across phytoplankton and prokaryotes. The three circles of each radar chart correspond to phylogenetic heritabilities of 0, 0.5, and 1. Mean phylogenetic heritability estimates are shown in purple, whereas the 95% HPD intervals are in dark grey. Note that we transformed all TPC parameters so that their statistical distributions would be approximately Gaussian.

Partitioning of thermal sensitivity across the phylogeny

To understand why thermal sensitivity has an intermediate phylogenetic heritability, we examined how clades throughout the phylogeny explore the parameter space (of E and W_{op}) using a disparity-through-time analysis [31,32]. At each branching point of the phylogeny, mean subclade disparity is calculated as the average squared Euclidean distance among trait values within the subclades, normalised to the disparity of trait values across the entire tree. The resulting disparity line is then compared to the null expectation, i.e., an envelope of disparities obtained from simulations of random evolution on the same tree. Through the comparison of the true trait disparity with the null expectation, it is possible to identify the exact periods of evolutionary time during which mean subclade disparity is higher or lower than expected under random evolution. Higher than expected subclade disparity indicates that clades converge in trait space, whereas lower than expected subclade disparity indicates that clades occupy distinct areas of parameter space (adaptive radiation) due to a deceleration of the evolutionary rate.

The mean subclade disparity of thermal sensitivity measures was higher than expected near the present, highlighting an increasing overlap in the parameter space of thermal sensitivity among distinct clades (Figs. 3 and S8). This pattern of increasing clade-wide convergence in thermal sensitivity is also apparent when comparing the thermal sensitivity distributions of different phyla (Figs. 4 and S3). For example, E and W_{op} are similarly distributed among Proteobacteria and Bacillariophyta despite the long evolutionary distance that separates them. This high convergence in thermal sensitivity space by diverse lineages suggests that variation in the two TPC parameters is mainly driven by adaptation to local environmental conditions, irrespective of species' evolutionary history. In other words, it is likely that particular thermal strategies (e.g., having low thermal sensitivity) may yield significant fitness gains at certain

environments (e.g., those with more temperature fluctuations), leading to convergent evolution of thermal sensitivity.

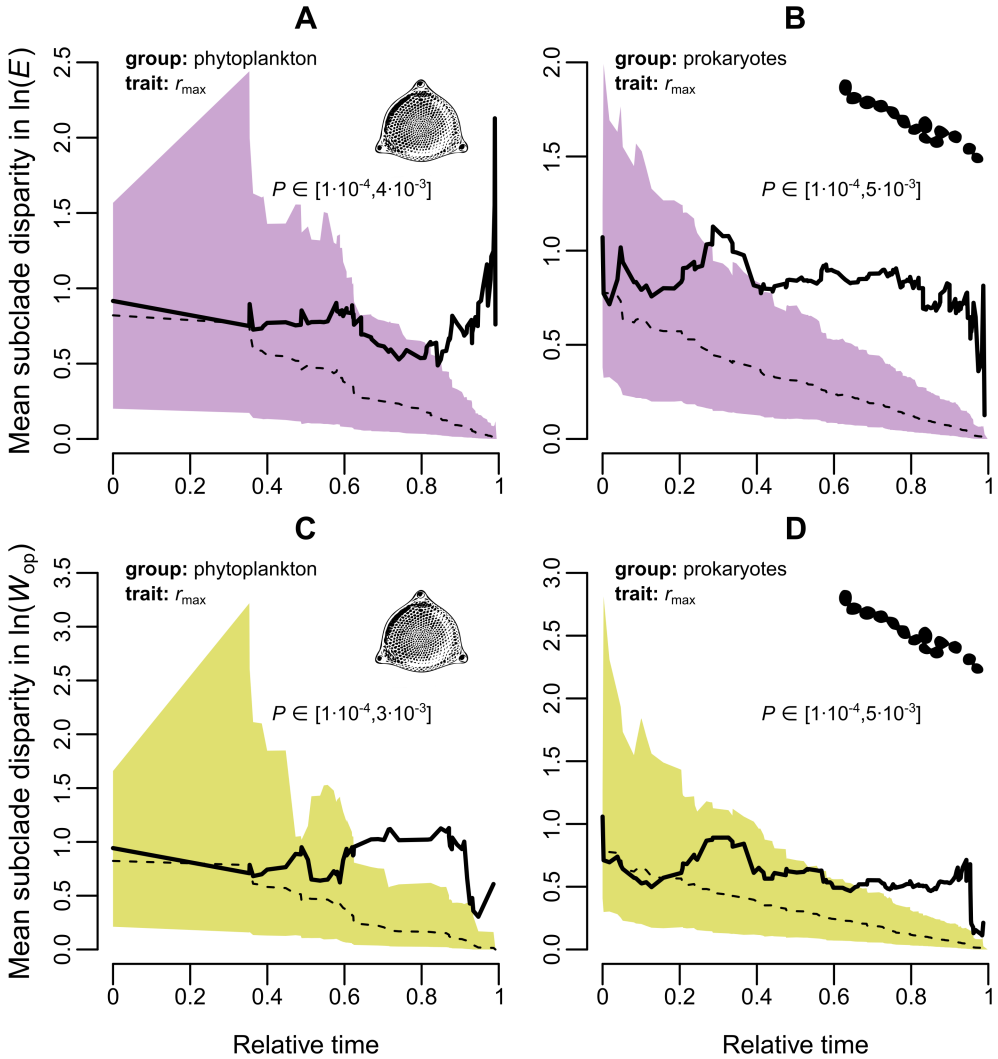

Fig 3. Change in mean subclade disparity in thermal sensitivity through time. Shaded regions represent the 95% confidence interval of the resulting trait disparity from 10,000 simulations of random Brownian evolution on each respective subtree. The dashed line stands for the median disparity across simulations, whereas the solid line is the observed trait disparity. The latter is plotted from the root of the tree ($t = 0$) until the most recent internal node. The reported P-values were obtained from the rank envelope test, whose null hypothesis is that the trait undergoes random evolution. Note that instead of a single value, a range of P-values is produced for each panel, due to the existence of ties. In general, species from evolutionarily remote clades tend to increasingly overlap in thermal sensitivity space (mean subclade disparity exceeds that expected under random evolution) with time.

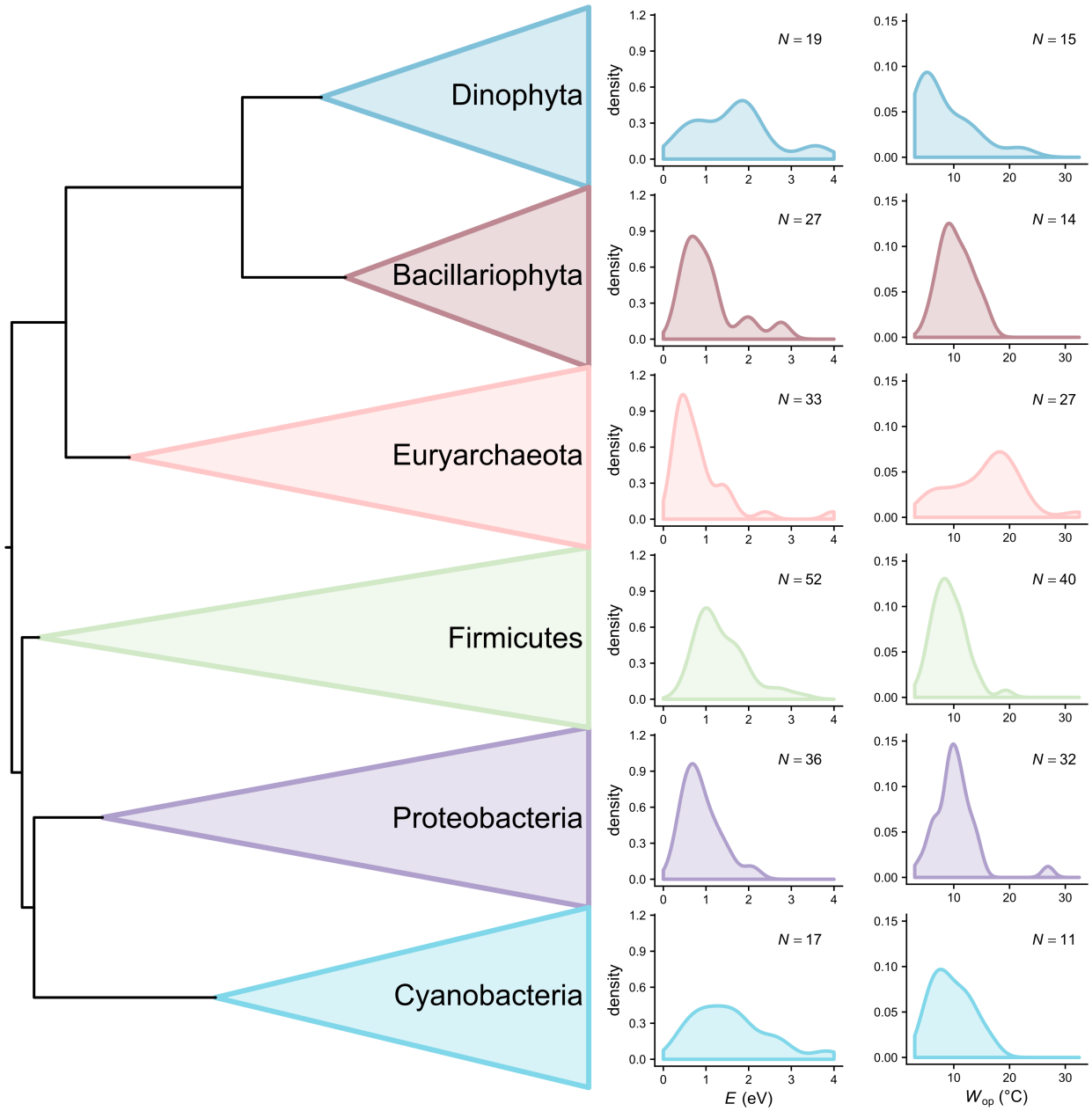

Fig 4. Distributions of thermal sensitivity estimates of $r_{\mathbf{max}}$ for the largest (most species-rich) phyla of this study. In general, more variation can be observed within than among phyla.

Mapping the evolutionary rate on the phylogeny

We estimated the evolutionary rate of thermal sensitivity measures for each branch of the phylogeny by fitting two extensions of the Brownian motion model: the free model [33] and the stable model [34]. Under the free model, the trait undergoes random evolution but with an evolutionary rate that varies across branches. The stable model can be seen as a generalisation of the free model, as the evolutionary change in trait values is sampled from a heavy-tailed stable distribution, of which the Gaussian distribution (assumed under Brownian motion) is a special case. Thus, the stable model should provide a more accurate representation of evolutionary rate variation, as it is better able to accommodate jumps in parameter space towards rare and extreme trait values.

The results were robust to the choice of model used for inferring evolutionary rates (Figs. 5 and S5). Rate shifts tend to occur sporadically throughout the phylogeny and especially in late-branching lineages, without being limited to particular clades. This pattern suggests that there is little variation in the evolutionary rate of thermal sensitivity among clades, with sudden bursts of trait evolution arising in parallel across evolutionarily remote lineages.

Visualization of trait evolution as a function of time, and test for directional selection

To further describe the evolution of thermal sensitivity, we visualized the E and W_{op} values from the root of each subtree until the present day, across all four TPC datasets. Ancestral states – and the uncertainty around them – were obtained from fits of the stable model of trait evolution, as described in the previous subsection. To also test the MTE expectation of a global (thermodynamically-constrained) optimum around 0.65 eV (or 0.32 eV) for E, and to simultaneously identify any putative directional trend towards lower (or higher) thermal sensitivity, we used the following model:

$$\ln(E) \sim \ln(\widehat{\theta}) + \mathrm{slope} \cdot t. \tag{2}$$

$\ln(E)$ values (those from extant species and ancestral states inferred with the stable model) were regressed against a global optimum ($\ln(\widehat{\theta})$) and a slope that captures a putative linear trend towards lower/higher values with relative time, t. The same model was also fitted to $\ln(W_{\mathrm{op}})$. The regressions were performed with MCMCglmm and were corrected for phylogeny as this resulted in lower Deviance Information Criterion (DIC) [35] values than those obtained from non-phylogenetic variants of the models. More precisely, we executed two MCMCglmm chains per regression for a million generations, sampling every thousand generations after the first hundred thousand.

This analysis (Fig. 6) did not provide support for thermal sensitivity evolving very tightly around a single global optimum. Instead, lineages explore large parts of the parameter space, often moving rapidly towards the upper and lower bounds (i.e., 0 and 4 eV), without reverting back to the presumed optimum (e.g., see the clade denoted by the arrow in Fig. 6D). The estimated optima for E of the two $r_{\max}$ datasets were much higher than the MTE expectation and, in the case of prokaryotes (Fig. 6B), the 95% HPD interval did not include 0.65. Similarly, the inferred optimum values for E of net photosynthesis rate and respiration rate (0.52 eV and 2.06 eV respectively; Fig. S9A,B) were both higher than 0.32 and 0.65 eV. The slope parameter that would capture the effects of directional selection in thermal sensitivity was not statistically different from zero for any dataset.

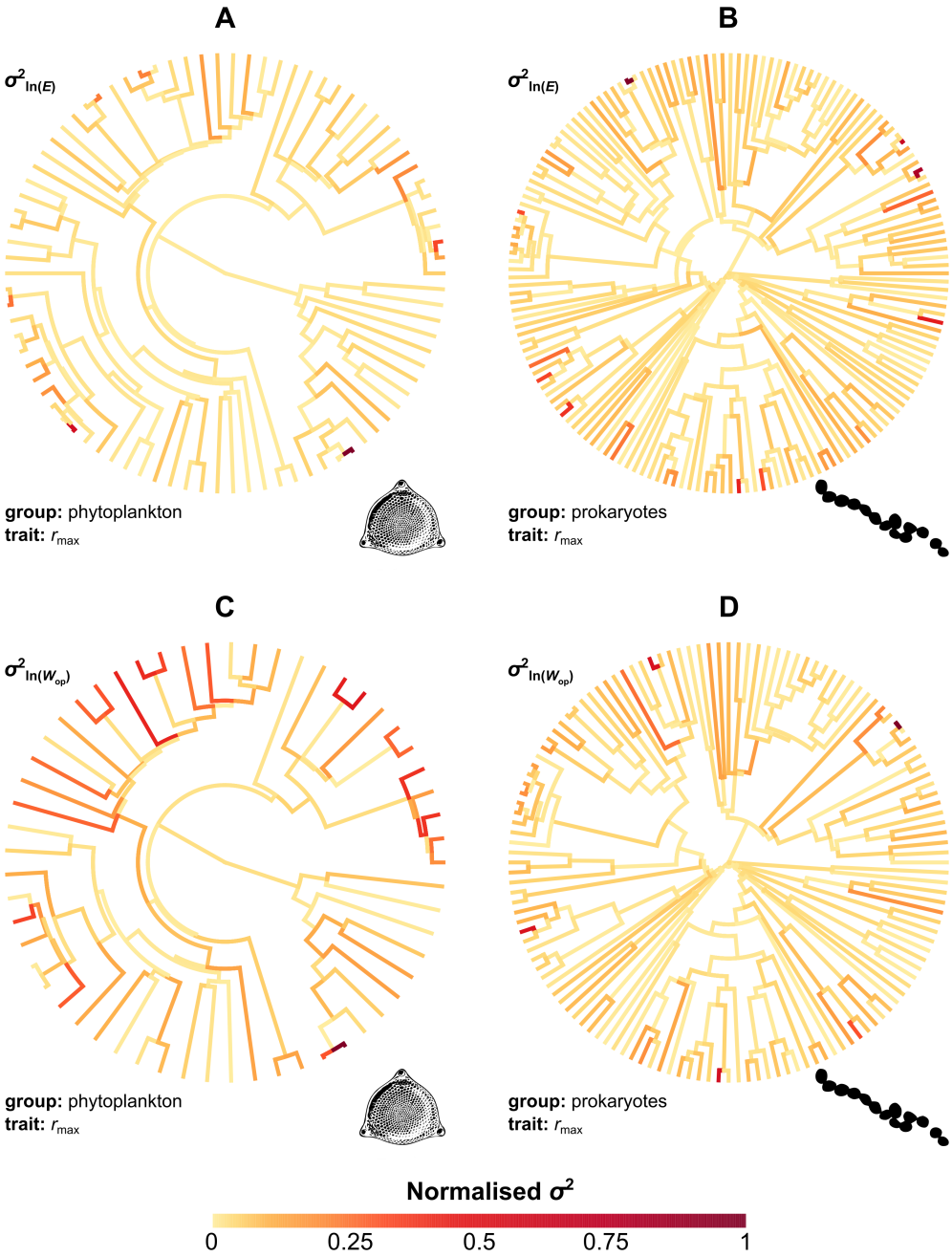

Fig 5. Variation in the evolutionary rate of thermal sensitivity across the phylogeny. Rates were estimated by fitting the stable model of trait evolution to each dataset and were then normalised between 0 and 1. Most branches exhibit relatively low rates of evolution (orange), whereas the highest rates (red and brown) are generally observed in late-branching lineages across different clades.

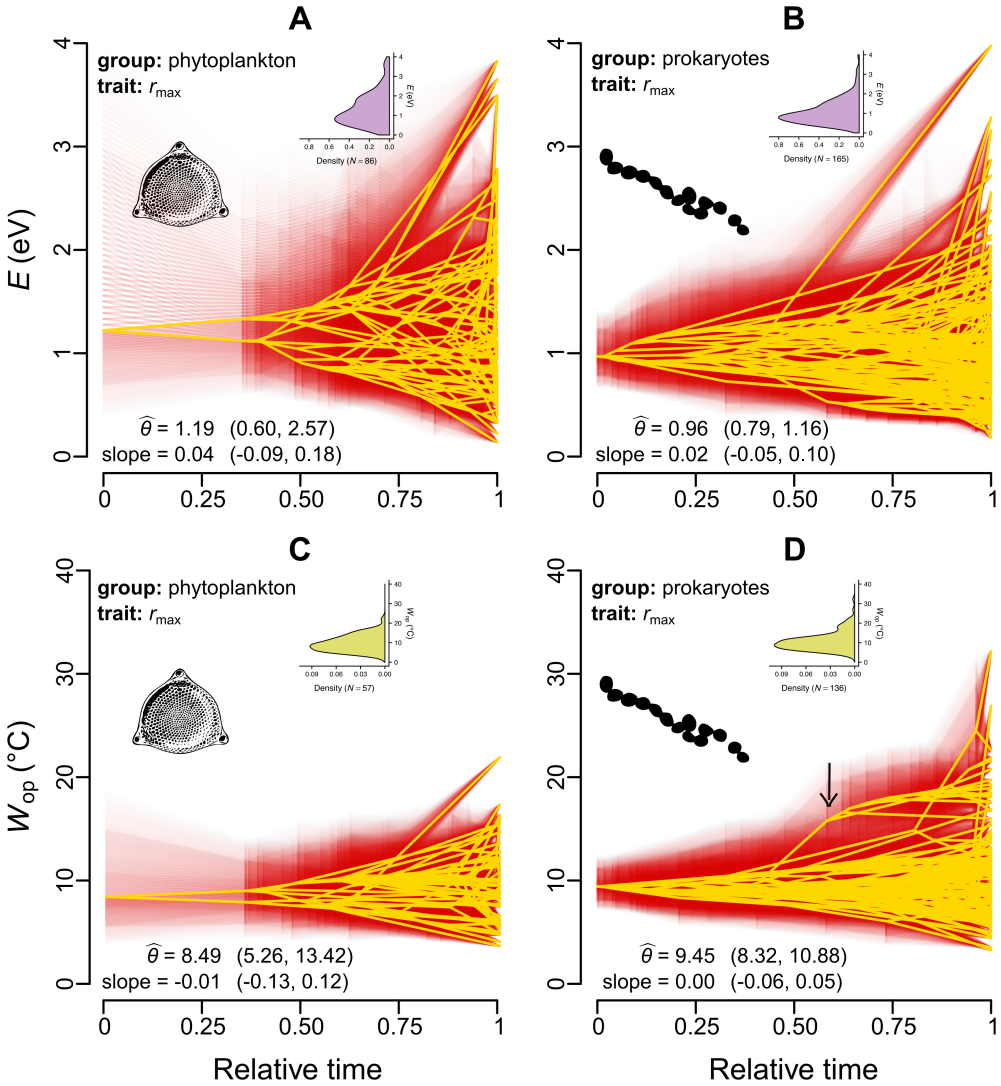

Fig 6. Projection of the phylogeny into thermal sensitivity versus time space. The values of ancestral nodes were estimated from fits of the stable model. Yellow lines represent the median estimates, whereas the 95% credible intervals are shown in red. $\widehat{\theta}$ is the estimated global optimum for each panel, whereas the existence of a linear trend towards lower/higher values is captured by the reported slope. Parentheses stand for the 95% HPD intervals for $\widehat{\theta}$ and the slope. All estimates were obtained for $\ln(E)$ and $\ln(W_{\text{op}})$, but the parameters are shown here in linear scale. The inset figures show the density distributions of E and W_{op} values of extant species in the dataset. The arrow in panel D shows an example of a whole clade shifting towards high W_{op} values, without being attracted back to $\widehat{\theta}$.

Latitudinally structured variation in thermal sensitivity

All our analyses so far converge on one conclusion: that the evolution of the thermal sensitivities of fitness-related traits can be rapid and largely independent of the evolutionary history of each lineage. This suggests that certain environments may select for particular values of thermal sensitivity. To identify environmental adaptation in thermal sensitivity, we tested for latitudinal variation in it using the combination of all four TPC datasets. Specifically, the increase in temperature fluctuations from low to intermediate absolute latitudes is expected to increasingly select for thermal generalists (lower E and higher W_{op} values) [3, 36, 37]. At high latitudes, however, temperature fluctuations may further increase or progressively decrease, depending on environment type (marine versus terrestrial) and differences between the two hemispheres [3, 36, 37]. In any case, the overwhelming majority of our thermal sensitivity estimates belonged to species/strains from low and intermediate latitudes (Fig. S10), enabling us to investigate the hypothesized gradual transition towards lower thermal sensitivity from the equator to intermediate latitudes.

Latitude indeed explained a significant amount of variation in E (which declined as expected) but not in W_{op} (Figs. 7 and S11, Tables S1 and S2). The E estimates of r_{max}, net photosynthesis rate, and respiration rate differed statistically in their intercepts but not in their slopes against latitude, although the latter could be an artefact of the small sample size. This result suggests that latitude could influence the E values of not only r_{max} but also other traits across various species groups. Dividing latitude into three bins (i.e., low, intermediate, and high absolute latitudes) and comparing their E distributions yielded similar conclusions (Fig. S12, Table S3).

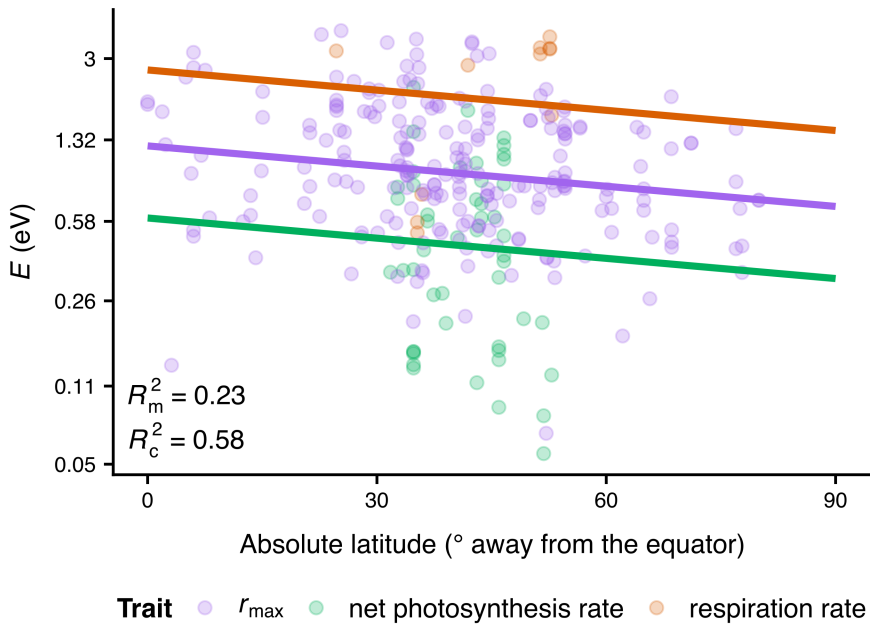

Fig 7. E values weakly decrease with absolute latitude. 23% of the variance is explained by latitude and trait identity, which increases to 58% if species identity is added as a random effect on the intercept. Note that values on the vertical axis increase exponentially.

Discussion

In this study, we have performed a thorough analysis of the evolution of the thermal sensitivities of $r_{\max}$ and its two key underlying physiological traits in plants (net photosynthesis rate and respiration rate). Our aim was to understand if thermal sensitivity varies in a random and non-adaptive way across species or if its distribution is shaped by selection. The former hypothesis was first introduced in early papers that described the Metabolic Theory of Ecology [6–8] and is based on the assumption that the performance of physiological traits (e.g., photosynthesis, respiration) [7, 10] and emergent proxies for fitness (such as $r_{\max}$) [38, 39] is directly determined by the activity of a single key rate-limiting enzyme (Universal Temperature Dependence).

In contrast to the UTD expectation, we detected substantial variation in thermal sensitivity, within and across traits and species groups (Fig. S2 in the S1 Appendix). Across phytoplankton and prokaryotes, in particular, we also found that thermal sensitivity was phylogenetically heritable (Fig. 2). Further analyses revealed that the evolution of thermal sensitivity is characterised by an increasing overlap in parameter space by evolutionarily remote lineages (Figs. 3 and 4) due to bursts of rapid evolution (Fig. 5). Additionally, visualisation of thermal sensitivity evolution through time (Figs. 6 and S9) did not provide evidence for a strongly-attracting global optimum in thermal sensitivity, which would be set by thermodynamic constraints and would prevent large shifts away from it (e.g., see the arrow in Fig. 6D).

Lastly, we identified a systematic relationship between E and latitude, likely driven by the increase in temperature fluctuations from the equator to intermediate latitudes. This result agrees with the expectation that thermally-variable environments should select for phenotypes with low thermal sensitivity, and vice versa [3, 17, 22]. That a similar latitudinal effect could not be detected on W_{op} is possibly because of the much smaller sample size available for this, combined with the fact that W_{op} is nonlinearly related to E (Fig. S4). In any case, E is arguably a more meaningful measure of niche width than W_{op} because the latter assumes that species mainly experience temperatures close to T_{pk}, while E captures the entire rise of the TPC. Besides temperature fluctuations, a decrease in E with absolute latitude could also be explained by the metabolic cold adaptation hypothesis [40–43]. According to it, cold-adapted species should evolve lower thermal sensitivities (as well as higher B_0 values; see Fig. 1) to maintain sufficient trait performance at very low temperatures. While our datasets do not possess the necessary resolution (especially at high latitudes; Figs. S10 and S12) for differentiating between these two alternative (and non-mutually exclusive) processes, this question remains to be addressed by future research.

Overall, a set of novel mechanistic explanations of TPC evolution emerge from our comparison of phylogenetic heritabilities of TPC parameters (Fig. 2). Contrary to E and W_{op}, which have intermediate phylogenetic heritabilities, T_{pk} is almost perfectly phylogenetically heritable and evolves relatively gradually (i.e., without large jumps in parameter space; see Fig. S6 in the S1 Appendix). Thus, we expect TPCs to adapt to different thermal environments through both gradual changes in T_{pk} and discontinuous changes in E. Gradual changes in T_{pk} may be achieved through evolutionary shifts in the melting temperature of enzymes, i.e., the temperature at which 50% of the enzyme population is deactivated [44, 45]. In contrast, changes in thermal sensitivity may be the outcome of i) evolution of enzymes with different heat capacities [45–47], ii) changes in the plasticity of cellular membranes [3, 48], or even iii) restructuring of the underlying metabolic network [49].

Fundamental differences in the selection mechanisms underlying the evolution of T_{pk} and E may also explain the difference in evolutionary patterns between them. Specifically, while these two TPC parameters are both associated with latitude, the former responds to mean environmental temperature [28, 50], whereas the latter to

temperature fluctuations [3, 17, 22, 23, 28]. We hypothesize that a species adapted to low temperatures is unlikely to adapt to a high-temperature environment rapidly enough (i.e., through a large increase in T_{pk}) as it is pushed to its thermal tolerance limits [51, 52]. In contrast, a species adapted to a fluctuating thermal environment (i.e., with a low E value) should be able to survive in more thermally stable conditions without much cost, becoming a thermal specialist (i.e., with a high E value) relatively rapidly, resulting in the observed jumps in trait space when mapped on the phylogeny (Figs. 3, 6, S8, and S9). Nevertheless, latitude, trait identity, and species identity account for only 58% of the variance in E (Fig. 7), indicating that shifts in E may also be driven by other factors such as biotic interactions [15, 53, 54]. A systematic identification of drivers of thermal sensitivity as well as the magnitude of their respective influence could be the focus of future studies.

For the thermal sensitivity of $r_{\max}$ in particular, the observed patterns of discontinuous evolution likely reflect the evolution of TPCs of underlying physiological traits on which it depends. For example, in populations of photosynthetic cells, shifts in the thermal sensitivity of any or all of photosynthesis rate, respiration rate and carbon allocation efficiency can induce large changes in the E of $r_{\max}$ [27]. Indeed, we observed large adaptive shifts in thermal sensitivity even for fundamental physiological traits such as respiration rate (Fig. S9B,D), contrary to the MTE expectation of strong evolutionary conservatism [6–8]. It remains to be seen whether this pattern is driven by a similar lack of evolutionary conservation e.g., in the shape of the thermal stability curves [45] of enzymes involved in metabolic reactions. Further research is clearly also needed on how the thermal sensitivities of different traits underlying fitness interact, and the extent to which these interactions can be modified through adaptation.

Besides biological-driven variation in thermal sensitivity, "artificial" variation may also be present, hindering the recognition of real patterns. For example, E estimates can be inaccurate if trait measurements in the rise of the TPC are limited, and span too narrow a range of temperatures [18]. To address this issue, we only kept E estimates if at least four trait measurements were available at the rise of each TPC. Further variation in thermal sensitivity can be introduced if trait values are measured instantaneously (without allowing sufficient time for acclimation) or under suboptimal conditions (e.g., under nutrient- or light-deficient conditions). Such treatments can lead to systematic biases in the shape of the resulting TPCs, which may strongly differ from TPCs obtained after adequate acclimation and under optimal growth conditions [24, 55–58]. To avoid such biases, the datasets that we used only included TPCs that were experimentally determined after acclimation and under optimal conditions.

Put together, all these results yield a compelling mechanistic explanation of how evolution shapes the distribution of E, and emphasize the need to consider the ecological and evolutionary underpinnings as well as implications of variation in E, as has been pointed out in a spate of recent studies [15, 17, 18, 27]. In particular, our study helps explain the reason for the right skewness in the E distributions previously identified across practically all traits and taxonomic groups [15, 17, 18]. A clear explanation for this pattern was previously lacking, partly because MTE posits that E should be thermodynamically constrained and thus almost invariable across species [6–8]. Our study fills this gap in understanding by showing that the distribution of E is the outcome of frequent convergent evolution, driven by the adaptation of species from different clades to similar environmental conditions. In other words, as species encounter new environments through active or passive dispersal [59–61], they face selection for particular values of thermal sensitivity, which results in (often large) shifts in E. This process explains both the low variation in E among species groups (Fig. 4) and the shape of its distribution. More precisely, the high degree of right

skewness probably reflects the fact that most environments select for thermal generalists, with high E values being less frequently advantageous. Our findings have implications for ecophysiological models which may benefit from accounting for variation in thermal sensitivity among species or individuals. This could both yield an improved fit to empirical datasets [62] and provide a more realistic approximation of the processes being studied. Finally, the existence of adaptive variation in thermal sensitivity is likely to partly drive ecological patterns at higher scales (e.g., the response of an ecosystem to warming). How differences in thermal sensitivity among species influence ecosystem function is largely unaddressed [29, 62] but highly important for accurately predicting the impacts of climate change on diverse ecosystems.

Methods

Phylogeny reconstruction and relative time calibration

We performed sequence alignment using MAFFT (v. 7.123b) [63] and its L-INS-i algorithm, and ran Noisy (v. 1.5.12) [64] with the default options to identify and remove phylogenetically uninformative homoplastic sites. For a more robust phylogenetic reconstruction, we used the results of previous phylogenetic studies by extracting the Open Tree of Life [65] topology for the species in our dataset using the rotl R package [66]. We manually examined the topology to eliminate any obvious errors. In total, 497 species were present in the tree, whereas many nodes were polytomic. To add missing species and resolve polytomies, we inferred 1,500 trees with RAxML (v. 8.2.9) [67] from our concatenated sequence alignment, using the Open Tree of Life topology as a backbone constraint and the General Time-Reversible model [68] with Γ-distributed rate variation among sites [69]. This model was fitted separately to each gene partition (i.e., one partition for the alignment of the small subunit rRNA gene sequences and one partition for the alignment of cbbL/rbcL gene sequences). Out of the 1,500 resulting tree topologies, we selected the tree with the highest log-likelihood and performed bootstrapping (using the extended majority-rule criterion) [70] to evaluate the statistical support for each node.

Finally, we calibrated the resulting RAxML tree to units of relative time by running DPPDiv [71] on the alignment of the small subunit rRNA gene sequences using the uncorrelated Γ-distributed rates model [72] (Fig. S1 in the S1 Appendix). For this, we used the alignment of small subunit rRNA gene sequences only, as DPPDiv can only be run on a single gene partition. We executed two DPPDiv runs for 9.5 million generations, sampling from the posterior distribution every 100 generations. After discarding the first 25% of samples as burn-in, we ensured that the two runs had converged on statistically indistinguishable posterior distributions by examining the effective sample size and the potential scale reduction factor [73, 74] for all model parameters. More precisely, we verified that all parameters had an effective sample size above 200 and a potential scale reduction factor value below 1.1. To summarise the posterior distribution of calibrated trees into a single relative chronogram, we kept 4,750 trees per run (one tree every 1,500 generations) and calculated the median height for each node using the TreeAnnotator program [75].

Sharpe-Schoolfield model fitting

To obtain estimates of the parameters of each experimentally determined TPC, we fitted the following four-parameter variant of the Sharpe-Schoolfield model (Fig. 1) [5, 28]:

$$B(T) = B_0 \cdot \frac{e^{\left[\frac{-E}{k}\cdot\left(\frac{1}{T}-\frac{1}{T_{\mathrm{ref}}}\right)\right]}}{1+\frac{E}{E_{\mathrm{D}}-E}\cdot e^{\left[\frac{E_{\mathrm{D}}}{k}\cdot\left(\frac{1}{T_{\mathrm{pk}}}-\frac{1}{T}\right)\right]}}. \quad (3)$$

This model extends the Boltzmann-Arrhenius model (Eq. 1) to capture the decline in trait performance after the TPC reaches its peak (T_{pk}). We followed the same approach for fitting the Sharpe-Schoolfield model as in reference [28]. Briefly, we set T_{ref} to 0°C, as for B_0 to be biologically meaningful (see Fig. 1), it needs to be normalised at a temperature below the minimum T_{pk} in the study. Thus, a T_{ref} value of 0°C allowed us to include TPCs from species with low T_{pk} values in the analyses. Also, as certain specific TPC parameter combinations can mathematically lead to an overestimation of B_0 compared to the true value, $B(T_{\mathrm{ref}})$ [76], we manually recalculated $B(T_{\mathrm{ref}})$ for each TPC after obtaining estimates of the four main parameters (B_0, E, T_{pk}, and E_{D}). For simplicity, these recalculated $B(T_{\mathrm{ref}})$ values are referred to as B_0 throughout the study. Finally, B_{pk} and W_{op} were calculated based on the estimates of the four main parameters.

After rejecting fits with an R^2 below 0.5, there were i) 312 fits across 118 species from the phytoplankton $r_{\max}$ dataset, ii) 289 fits across 189 species from the prokaryote $r_{\max}$ dataset, iii) 87 fits across 38 species from the net photosynthesis rates dataset, and iv) 34 fits across 18 species from the respiration rates dataset. Note that some species were represented by multiple fits due to the inclusion of experimentally-determined TPCs from different strains of the same species or from different geographical locations. To ensure that all TPC parameters were reliably estimated, we performed further filtering based on the following criteria: i) B_0 and E estimates were rejected if fewer than four experimental data points were available below T_{pk}. ii) Extremely high E estimates (i.e., above 4 eV) were rejected. iii) W_{op} values were retained if at least four data points were available below T_{pk} and two after it. iv) Two data points below and after the peak were required for accepting the estimates of T_{pk} and B_{pk}. v) E_{D} estimates were kept if at least four data points were available at temperatures greater than T_{pk}.

Estimation of phylogenetic heritability for all TPC parameters

As in the previous subsection, the methodology that we used here was identical to that in reference [28]. In short, we specified a phylogenetic mixed-effects model for each of the two large TPC datasets with MCMCglmm. The models had a combined response with all TPC parameters transformed towards normality. The uncertainty for each estimate was obtained with the delta method [77] or via bootstrapping (for $\ln(W_{\mathrm{op}})$) and was incorporated into the model. Missing estimates in the response variables (i.e., when not all parameter estimates could be obtained for the same TPC) were modelled according to the "Missing At Random" approach [30, 78]. Regarding fixed effects, a separate intercept was specified for each TPC parameter. Species identity was treated as a random effect on the intercepts and was corrected for phylogeny through the integration of the inverse of the phylogenetic variance-covariance matrix. For each dataset, two Markov chain Monte Carlo chains were run for 200 million generations and estimates of the parameters of the model were sampled every 1,000 generations after the first 20 million generations were discarded as burn-in. Tests to ensure that the chains had converged and that the parameters were adequately sampled were done as previously described.

Disparity-through-time analyses

We performed disparity-through-time analyses for $\ln(E)$ and $\ln(W_{\mathrm{op}})$, using the rank envelope method [32] to generate a confidence envelope from 10,000 simulations of random evolution. As it is not straightforward to incorporate multiple measurements per species with this method, we selected the $\ln(E)$ or $\ln(W_{\mathrm{op}})$ estimate of the Sharpe-Schoolfield model fit with the highest R^2 value per species.

Free and stable model fitting

We fitted the free and the stable models of trait evolution to estimates of $\ln(E)$ and $\ln(W_{\mathrm{op}})$, using the motmot.2.0 R package (v. 1.1.2) [79, 80] and the stabletraits software [34] respectively. To obtain each fit of the stable model, we executed four independent Markov chain Monte Carlo chains for 30 million generations, recording posterior parameter samples every 100 generations. Samples from the first 7.5 million generations were excluded, whereas the remaining samples were examined to ensure that convergence had been achieved.

Investigation of a putative relationship between latitude and $\ln(E)$ and $\ln(W_{\mathrm{op}})$

We examined the relationship of thermal sensitivity with latitude by fitting regression models with MCMCglmm to all four TPC datasets combined. The response variable was $\ln(E)$ or $\ln(W_{\mathrm{op}})$, whereas possible predictor variables were i) latitude (in radian units and using a cosine transformation, as absolute latitude in degree units, or split in three bins of low, intermediate, and high absolute latitude; subsections S4.2 and S4.3 in the S1 Appendix), ii) the trait from which thermal sensitivity estimates were obtained, and iii) the interaction between latitude and trait identity. To properly incorporate multiple measurements from the same species (where available), we treated species identity as a random effect on the intercept. We fitted both phylogenetic and non-phylogenetic variants of all candidate models. Two chains per model were run for five million generations each, with samples from the posterior being captured every thousand generations. We verified that each pair of chains had sufficiently converged, after discarding samples from the first 500,000 generations. To identify the most appropriate model, we first rejected models that had a non-intercept coefficient with a 95% Highest Posterior Density (HPD) interval that included zero. We then selected the model with the lowest mean DIC value. To report the proportions of variance explained by the fixed effects ($\mathrm{Var}_{\mathrm{fixed}}$), by the random effect ($\mathrm{Var}_{\mathrm{random}}$), or left unexplained ($\mathrm{Var}_{\mathrm{resid}}$), we calculated the marginal and conditional coefficients of determination [81]:

$$R^2_{\mathrm{m}} = \frac{\mathrm{Var}_{\mathrm{fixed}}}{\mathrm{Var}_{\mathrm{fixed}} + \mathrm{Var}_{\mathrm{random}} + \mathrm{Var}_{\mathrm{resid}}}, \tag{4}$$

$$R^2_{\mathrm{c}} = \frac{\mathrm{Var}_{\mathrm{fixed}} + \mathrm{Var}_{\mathrm{random}}}{\mathrm{Var}_{\mathrm{fixed}} + \mathrm{Var}_{\mathrm{random}} + \mathrm{Var}_{\mathrm{resid}}}. \tag{5}$$

Supporting information

S1 Appendix.

Acknowledgments

We thank Iain Colin Prentice for providing comments on an early version of the manuscript. We are also grateful to James Rosindell, Jonathan Lloyd, Guy Woodward, and Andrew G. Hirst for valuable discussions, and to the CIPRES Science Gateway [82] for access to computational resources. Species silhouettes were obtained from phylopic.org and are used under the Public Domain license. The images of species in Fig. 1 were graciously provided by Eric Erbe, Christopher Pooley, and the Rocky Mountain National Park, also under the Public Domain license. DGK was supported by a Natural Environment Research Council (NERC) Doctoral Training Partnership (DTP) scholarship (NE/L002515/1). TPS was supported by a Biotechnology and Biological Sciences Research Council (BBSRC) DTP scholarship (BB/J014575/1). SP was supported by NERC grants NE/M004740/1 and NE/M020843/1.

References

1. Collins M, Knutti R, Arblaster J, Dufresne JL, Fichefet T, Friedlingstein P, et al. Long-term Climate Change: Projections, Commitments and Irreversibility. In: Stocker TF, Qin D, Plattner GK, Tignor M, Allen SK, Boschung J, et al., editors. Climate Change 2013: The Physical Science Basis. Contribution of Working Group I to the Fifth Assessment Report of the Intergovernmental Panel on Climate Change. Cambridge, United Kingdom and New York, NY, USA: Cambridge University Press; 2013. p. 1029–1136.

2. Bathiany S, Dakos V, Scheffer M, Lenton TM. Climate models predict increasing temperature variability in poor countries. Sci Adv. 2018;4(5):eaar5809.

3. Angilletta MJ. Thermal adaptation: a theoretical and empirical synthesis. Oxford University Press; 2009.

4. Clarke A. Principles of Thermal Ecology: Temperature, Energy, and Life. Oxford University Press; 2017.

5. Schoolfield R, Sharpe P, Magnuson C. Non-linear regression of biological temperature-dependent rate models based on absolute reaction-rate theory. J Theor Biol. 1981;88(4):719–731.

6. Gillooly JF, Brown JH, West GB, Savage VM, Charnov EL. Effects of size and temperature on metabolic rate. Science. 2001;293(5538):2248–2251.

7. Brown JH, Gillooly JF, Allen AP, Savage VM, West GB. Toward a metabolic theory of ecology. Ecology. 2004;85(7):1771–1789.

8. Gillooly J, Allen A, Savage V, Charnov E, West G, Brown J. Response to Clarke and Fraser: effects of temperature on metabolic rate. Funct Ecol. 2006;20(2):400–404.

9. Corkrey R, Olley J, Ratkowsky D, McMeekin T, Ross T. Universality of thermodynamic constants governing biological growth rates. PLoS One. 2012;7(2):e32003.

10. Allen A, Gillooly J, Brown J. Linking the global carbon cycle to individual metabolism. Funct Ecol. 2005;19(2):202–213.

11. Clarke A, Fraser K. Why does metabolism scale with temperature? Funct Ecol. 2004;18(2):243–251.

12. Clarke A. Is there a universal temperature dependence of metabolism? Funct Ecol. 2004;18(2):252–256.

13. Clarke A. Temperature and the metabolic theory of ecology. Funct Ecol. 2006;20(2):405–412.

14. Farquhar GD, von Caemmerer S, Berry JA. A biochemical model of photosynthetic CO_2 assimilation in leaves of C_3 species. Planta. 1980;149(1):78–90.

15. Dell AI, Pawar S, Savage VM. Systematic variation in the temperature dependence of physiological and ecological traits. Proc Natl Acad Sci U S A. 2011;108(26):10591–10596.

16. Englund G, Öhlund G, Hein CL, Diehl S. Temperature dependence of the functional response. Ecol Lett. 2011;14(9):914–921.

17. Nilsson-Örtman V, Stoks R, De Block M, Johansson H, Johansson F. Latitudinally structured variation in the temperature dependence of damselfly growth rates. Ecol Lett. 2013;16(1):64–71.

18. Pawar S, Dell AI, Savage VM, Knies JL. Real versus artificial variation in the thermal sensitivity of biological traits. Am Nat. 2016;187(2):E41–E52.

19. Michaletz ST. Evaluating the kinetic basis of plant growth from organs to ecosystems. New Phytol. 2018;219(1):37–44.

20. Savva I, Bennett S, Roca G, Jordà G, Marbà N. Thermal tolerance of Mediterranean marine macrophytes: Vulnerability to global warming. Ecol Evol. 2018;8(23):12032–12043.

21. McShea DW. Mechanisms of large-scale evolutionary trends. Evolution. 1994;48(6):1747–1763.

22. Gilchrist GW. Specialists and generalists in changing environments. I. Fitness landscapes of thermal sensitivity. Am Nat. 1995;146(2):252–270.

23. Schaum CE, Buckling A, Smirnoff N, Studholme DJ, Yvon-Durocher G. Environmental fluctuations accelerate molecular evolution of thermal tolerance in a marine diatom. Nat Commun. 2018;9:1719.

24. Padfield D, Yvon-Durocher G, Buckling A, Jennings S, Yvon-Durocher G. Rapid evolution of metabolic traits explains thermal adaptation in phytoplankton. Ecol Lett. 2016;19(2):133–142.

25. Padfield D, Lowe C, Buckling A, Ffrench-Constant R, Student Research Team, Jennings S, et al. Metabolic compensation constrains the temperature dependence of gross primary production. Ecol Lett. 2017;20(10):1250–1260.

26. Schaum CE, Barton S, Bestion E, Buckling A, Garcia-Carreras B, Lopez P, et al. Adaptation of phytoplankton to a decade of experimental warming linked to increased photosynthesis. Nat Ecol Evol. 2017;1(4):0094.

27. García-Carreras B, Sal S, Padfield D, Kontopoulos DG, Bestion E, Schaum CE, et al. Role of carbon allocation efficiency in the temperature dependence of autotroph growth rates. Proc Natl Acad Sci U S A. 2018;115(31):E7361–E7368.

28. Kontopoulos DG, van Sebille E, Lange M, Yvon-Durocher G, Barraclough TG, Pawar S. Phytoplankton thermal responses adapt in the absence of hard thermodynamic constraints; 2018. Available from: bioRxiv:452250. Cited 4 June 2019.

29. Smith TP, Thomas TJH, García-Carreras B, Sal S, Yvon-Durocher G, Bell T, et al. Community-level respiration of prokaryotic microbes may rise with global warming. Nat Commun. 2019;10(1):1–11.

30. Hadfield JD. MCMC Methods for Multi-Response Generalized Linear Mixed Models: The MCMCglmm R Package. J Stat Softw. 2010;33(2):1–22.

31. Harmon LJ, Schulte JA, Larson A, Losos JB. Tempo and mode of evolutionary radiation in iguanian lizards. Science. 2003;301(5635):961–964.

32. Murrell DJ. A global envelope test to detect non-random bursts of trait evolution. Methods Ecol Evol. 2018;9(7):1739–1748.

33. Mooers AØ, Vamosi SM, Schluter D. Using phylogenies to test macroevolutionary hypotheses of trait evolution in cranes (Gruinae). Am Nat. 1999;154(2):249–259.

34. Elliot MG, Mooers AØ. Inferring ancestral states without assuming neutrality or gradualism using a stable model of continuous character evolution. BMC Evol Biol. 2014;14(1):226.

35. Spiegelhalter DJ, Best NG, Carlin BP, van der Linde A. Bayesian measures of model complexity and fit. J R Stat Soc Series B Stat Methodol. 2002;64(4):583–639.

36. Vasseur DA, Yodzis P. The color of environmental noise. Ecology. 2004;85(4):1146–1152.

37. Clarke A, Gaston KJ. Climate, energy and diversity. Proc Biol Sci. 2006;273(1599):2257–2266.

38. Savage VM, Gillooly JF, Brown JH, West GB, Charnov EL. Effects of body size and temperature on population growth. Am Nat. 2004;163(3):429–441.

39. Frazier MR, Huey RB, Berrigan D. Thermodynamics constrains the evolution of insect population growth rates: "warmer is better". Am Nat. 2006;168(4):512–520.

40. Wohlschlag DE. Metabolism of an Antarctic fish and the phenomenon of cold adaptation. Ecology. 1960;41(2):287–292.

41. Clarke A. Seasonal acclimatization and latitudinal compensation in metabolism: do they exist? Funct Ecol. 1993;7(2):139–149.

42. Chown SL, Haupt TM, Sinclair BJ. Similar metabolic rate-temperature relationships after acclimation at constant and fluctuating temperatures in caterpillars of a sub-Antarctic moth. J Insect Physiol. 2016;85:10–16.

43. Payne NL, Smith JA. An alternative explanation for global trends in thermal tolerance. Ecol Lett. 2017;20(1):70–77.

44. Somero GN. Proteins and temperature. Annu Rev Physiol. 1995;57(1):43–68.

45. Pucci F, Rooman M. Physical and molecular bases of protein thermal stability and cold adaptation. Curr Opin Struct Biol. 2017;42:117–128.

46. Hobbs JK, Jiao W, Easter AD, Parker EJ, Schipper LA, Arcus VL. Change in heat capacity for enzyme catalysis determines temperature dependence of enzyme catalyzed rates. ACS Chem Biol. 2013;8(11):2388–2393.

47. DeLong JP, Gibert JP, Luhring TM, Bachman G, Reed B, Neyer A, et al. The combined effects of reactant kinetics and enzyme stability explain the temperature dependence of metabolic rates. Ecol Evol. 2017;7(11):3940–3950.

48. Cooper BS, Hammad LA, Montooth KL. Thermal adaptation of cellular membranes in natural populations of *Drosophila melanogaster*. Funct Ecol. 2014;28(4):886–894.

49. Braakman R, Follows MJ, Chisholm SW. Metabolic evolution and the self-organization of ecosystems. Proc Natl Acad Sci U S A. 2017;114(15):E3091–E3100.

50. Thomas MK, Kremer CT, Klausmeier CA, Litchman E. A global pattern of thermal adaptation in marine phytoplankton. Science. 2012;338(6110):1085–1088.

51. Araújo MB, Ferri-Yáñez F, Bozinovic F, Marquet PA, Valladares F, Chown SL. Heat freezes niche evolution. Ecol Lett. 2013;16(9):1206–1219.

52. Sunday J, Bennett JM, Calosi P, Clusella-Trullas S, Gravel S, Hargreaves AL, et al. Thermal tolerance patterns across latitude and elevation. Philos Trans R Soc Lond B Biol Sci. 2019;374(1778):20190036.

53. Dell AI, Pawar S, Savage VM. Temperature dependence of trophic interactions are driven by asymmetry of species responses and foraging strategy. J Anim Ecol. 2014;83(1):70–84.

54. Bestion E, García-Carreras B, Schaum CE, Pawar S, Yvon-Durocher G. Metabolic traits predict the effects of warming on phytoplankton competition. Ecol Lett. 2018;21(5):655–664.

55. Thomas MK, Aranguren-Gassis M, Kremer CT, Gould MR, Anderson K, Klausmeier CA, et al. Temperature–nutrient interactions exacerbate sensitivity to warming in phytoplankton. Glob Chang Biol. 2017;23:3269–3280.

56. Bestion E, Schaum CE, Yvon-Durocher G. Nutrient limitation constrains thermal tolerance in freshwater phytoplankton. Limnol Oceanogr Lett. 2018;3(6):436–443.

57. Rohr JR, Civitello DJ, Cohen JM, Roznik EA, Sinervo B, Dell AI. The complex drivers of thermal acclimation and breadth in ectotherms. Ecol Lett. 2018;21(9):1425–1439.

58. Wang H, Atkin OK, Keenan TF, Smith N, Wright IJ, Bloomfield KJ, et al.. Thermal acclimation of leaf respiration consistent with optimal plant function; 2018. Available from: bioRxiv:434084. Cited 4 June 2019.

59. Finlay BJ. Global dispersal of free-living microbial eukaryote species. Science. 2002;296(5570):1061–1063.

60. Tamames J, Abellán JJ, Pignatelli M, Camacho A, Moya A. Environmental distribution of prokaryotic taxa. BMC Microbiol. 2010;10(1):85.

61. Doblin MA, van Sebille E. Drift in ocean currents impacts intergenerational microbial exposure to temperature. Proc Natl Acad Sci U S A. 2016;113(20):5700–5705.

62. Johnston ASA, Sibly RM. The influence of soil communities on the temperature sensitivity of soil respiration. Nat Ecol Evol. 2018;2(10):1597–1602.

63. Katoh K, Standley DM. MAFFT multiple sequence alignment software version 7: improvements in performance and usability. Mol Biol Evol. 2013;30(4):772–780.

64. Dress AW, Flamm C, Fritzsch G, Grünewald S, Kruspe M, Prohaska SJ, et al. Noisy: identification of problematic columns in multiple sequence alignments. Algorithms Mol Biol. 2008;3(1):7.

65. Hinchliff CE, Smith SA, Allman JF, Burleigh JG, Chaudhary R, Coghill LM, et al. Synthesis of phylogeny and taxonomy into a comprehensive tree of life. P Natl Acad Sci USA. 2015;112(41):12764–12769.

66. Michonneau F, Brown JW, Winter DJ. rotl: an R package to interact with the Open Tree of Life data. Methods Ecol Evol. 2016;7(12):1476–1481.

67. Stamatakis A. RAxML version 8: a tool for phylogenetic analysis and post-analysis of large phylogenies. Bioinformatics. 2014;30(9):1312–1313.

68. Tavaré S. Some probabilistic and statistical problems in the analysis of DNA sequences. In: Miura RM, editor. Some Mathematical Questions in Biology: DNA Sequence Analysis. Providence (RI): American Mathematical Society; 1986. p. 57–86.

69. Gu X, Fu YX, Li WH. Maximum likelihood estimation of the heterogeneity of substitution rate among nucleotide sites. Mol Biol Evol. 1995;12(4):546–557.

70. Pattengale ND, Alipour M, Bininda-Emonds OR, Moret BM, Stamatakis A. How many bootstrap replicates are necessary? In: Annual International Conference on Research in Computational Molecular Biology. Springer; 2009. p. 184–200.

71. Heath TA, Holder MT, Huelsenbeck JP. A Dirichlet process prior for estimating lineage-specific substitution rates. Mol Biol Evol. 2012;29(3):939–955.

72. Drummond AJ, Ho SY, Phillips MJ, Rambaut A. Relaxed phylogenetics and dating with confidence. PLoS Biol. 2006;4(5):e88.

73. Gelman A, Rubin DB. Inference from iterative simulation using multiple sequences. Stat Sci. 1992;7(4):457–472.

74. Brooks SP, Gelman A. General methods for monitoring convergence of iterative simulations. J Comput Graph Stat. 1998;7(4):434–455.

75. Rambaut A, Drummond AJ. TreeAnnotator; 2018 [cited 30 November 2018]. Available from: `http://beast.community/treeannotator`.

76. Kontopoulos DG, García-Carreras B, Sal S, Smith TP, Pawar S. Use and misuse of temperature normalisation in meta-analyses of thermal responses of biological traits. PeerJ. 2018;6:e4363.

77. Oehlert GW. A note on the delta method. Am Stat. 1992;46(1):27–29.

78. Garamszegi LZ. Modern Phylogenetic Comparative Methods and Their Application in Evolutionary Biology: Concepts and Practice. Springer Berlin Heidelberg; 2014.

79. Thomas GH, Freckleton RP. MOTMOT: models of trait macroevolution on trees. Methods Ecol Evol. 2012;3(1):145–151.

80. Puttick M, Thomas G, Freckleton R, Ingram T, Orme D, Paradis E. motmot.2.0: Models of Trait Macroevolution on Trees; 2018.

81. Nakagawa S, Schielzeth H. A general and simple method for obtaining R^2 from generalized linear mixed-effects models. Methods Ecol Evol. 2013;4(2):133–142.

82. Miller MA, Pfeiffer W, Schwartz T. Creating the CIPRES Science Gateway for inference of large phylogenetic trees. In: Gateway Computing Environments Workshop (GCE), 2010. Ieee; 2010. p. 1–8.